Research Highlights (Required)

To create your highlights, please type the highlights against each `\item` command.

It should be short collection of bullet points that convey the core findings of the article. It should include 3 to 5 bullet points (maximum 85 characters, including spaces, per bullet point.)

- We propose an effective single-stage framework for multi-hand 3D reconstruction from a still image. To the best of our knowledge, we are the first to detect and recover the textured hand mesh simultaneously from images in the wild.

- Our method supports end-to-end training and has clear advantages over previous similar methods in terms of accuracy and inference speed. Besides, our single-stage framework requires no additional third-party detectors, making it easier to deploy.

- Both quantitative and qualitative results demonstrate the effectiveness of our proposed framework. Our method achieves the state-of-the-art performance under the weakly-supervised setting, which even outperforms several fully-supervised model-based methods.

Computer Vision and Image Understanding
journal homepage: www.elsevier.com

End-to-end Weakly-supervised Single-stage Multiple 3D Hand Mesh Reconstruction from a Single RGB Image

Jinwei Ren[a], Jianke Zhu[a,b,**], Jialiang Zhang[a]

[a]*School of Computer Science and Technology, Zhejiang University, 38 Zheda Road, Hangzhou 310000, China*
[b]*Alibaba-Zhejiang University Joint Research Institute of Frontier Technologies, Hangzhou 310000, China*

ABSTRACT

In this paper, we consider the challenging task of simultaneously locating and recovering multiple hands from a single 2D image. Previous studies either focus on single hand reconstruction or solve this problem in a multi-stage way. Moreover, the conventional two-stage pipeline firstly detects hand areas, and then estimates 3D hand pose from each cropped patch. To reduce the computational redundancy in preprocessing and feature extraction, for the first time, we propose a concise but efficient single-stage pipeline for multi-hand reconstruction. Specifically, we design a multi-head auto-encoder structure, where each head network shares the same feature map and outputs the hand center, pose and texture, respectively. Besides, we adopt a weakly-supervised scheme to alleviate the burden of expensive 3D real-world data annotations. To this end, we propose a series of losses optimized by a stage-wise training scheme, where a multi-hand dataset with 2D annotations is generated based on the publicly available single hand datasets. In order to further improve the accuracy of the weakly supervised model, we adopt several feature consistency constraints in both single and multiple hand settings. Specifically, the keypoints of each hand estimated from local features should be consistent with the re-projected points predicted from global features. Extensive experiments on public benchmarks including FreiHAND, HO3D, InterHand2.6M and RHD demonstrate that our method outperforms the state-of-the-art model-based methods in both weakly-supervised and fully-supervised manners. The code and models are available at `https://github.com/zijinxuxu/SMHR`.

1. Introduction

Recently, a surge of research efforts (Zimmermann et al., 2019; Hampali et al., 2020; Chen et al., 2021b) have been devoted to 3D hand reconstruction. In contrast to the conventional approaches relying on RGB-D sensor (Yuan et al., 2018) or multiple view geometry (Simon et al., 2017), recovering 3D hand pose and its shape from single color image is more challenging due to the ambiguities in depth and scale.

Most of existing methods mainly focus on the problem of recovering single hand only. However, human naturally uses both of their hands in daily life. In the scene of multi person interaction, such as shaking hands, playing chess, sign language and piano teaching, it is necessary to detect and recover the

pose of multiple hands at the same time. Hence, reconstructing multiple hands from a single image is a promising task that has not been extensively studied yet. In general, recovering multiple hands in an image is more difficult than reconstructing one hand. A straightforward solution is to decompose it into two separate parts. The hand region is firstly detected by the off-the-shelf object detector, which is further fed into a single hand regressor. However, this two-stage pipeline suffers from the problem of redundant feature extraction. Since it processes each hand instance individually, the overall computation cost grows linearly with the total number of hands in the image. Besides, the hand reconstruction heavily depends on the quality of the detector, which brings the uncertainty and inconvenience in the real-world application. In the case of multi-hand scenarios, the relative position in camera space is necessary for scene understanding and interaction analysis. However, the multi-stage model may only deal with the cropped and centered hand and

---

[**]Corresponding author.
  e-mail: `jkzhu@zju.edu.cn` (Jianke Zhu)
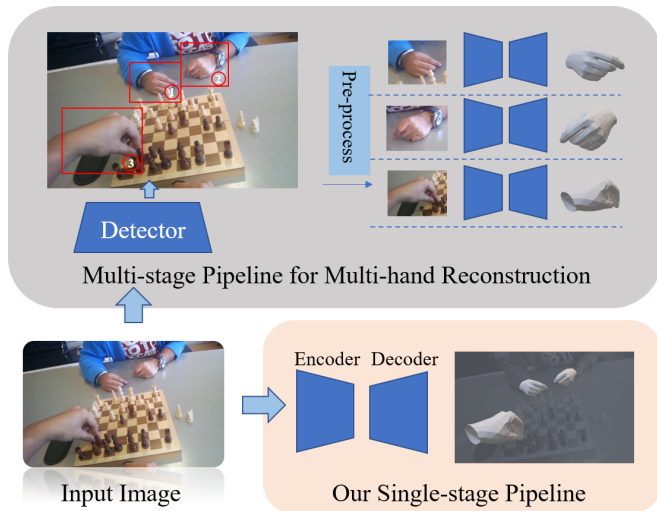
Fig. 1: Comparison of conventional multi-stage scheme and our single-stage pipeline. Our method avoids the redundant feature encoding process, which does not rely on the off-the-shelf hand detectors.

recover the relative pose in the model space.

To address the above limitations, we propose an efficient end-to-end weakly-supervised multiple 3D hand mesh reconstruction approach. Inspired by the single-stage object detection methods, such as CenterNet (Zhou et al., 2019) we integrate both hand center localization and mesh reconstruction within single network inference. There are some works adopt similar pipeline for multiple human face(Zhang et al., 2021) and body reconstruction (Sun et al., 2021; Zhang et al., 2022). However, the hand suffers from severe self-occlusions and complex articulations, which makes it more challenging for estimation. Besides, we need to additionally consider the problem of distinguishing between left and right hands instead of simply treating it as the center of the target. During the training period, a differentiable hybrid loss upon each hand center is employed to learn the decoupled hand model parameters and position jointly in an end-to-end manner. The comparison of our single-stage pipeline and conventional multi-stage scheme is depicted in Fig. 1.

Besides, it is extremely difficult to obtain the 3D labels for real-world image, especially in multiple hands scenarios. Methods requiring tedious and time-consuming iterative optimization and numerous fine-grained 3D labels are not friendly enough for the real-world applications. Transformer-based approach (Lin et al., 2021a,b) and GCN-based methods (Ge et al., 2019; Chen et al., 2021a) may not be suitable for this scenario, since they often require dense 3D supervision for all vertices and a coarse-to-fine refinement process. In contrast, the requirements of model-based method for 3D supervision are not so strict. Thus, we adopt a model-based method trained through purely weakly-supervised fashion to mitigate the dependence on the expensive 3D manual annotated data. We demonstrate our superior performance on single hand dataset FreiHAND (Zimmermann et al., 2019) and HO3D (Hampali et al., 2020), in both weakly-supervised and fully-supervised settings. For the two-handed case, we obtain comparable results with previous fully supervised methods on RHD (Zimmermann

and Brox, 2017) using only 2D supervision. For the first time, we introduce the multi-hand scenario which contains more than two hands in the same image. Since there is no such dataset publicly available, we generate a multi-hand dataset for training and evaluation.

Comparing to the previous multi-stage pipeline, our single-stage method benefits from the anchor-free scheme, which can effectively deal with occlusions, as (Sun et al., 2021) does. More importantly, our method has the advantages of fast inference and easy configuration in multi-hand scenarios, as it does not require multiple encodings and gets rid of the limitations of third-party detectors. Besides, the hand texture is important in applications such as augmented reality and virtual reality, which provides more expressive and useful mesh representation. Benefiting from the high scalability of the proposed framework, we can easily extend our model to estimate texture and lighting parameters.

From above all, our main contributions of this work can be summarized as follows:

(1) We propose an effective single-stage framework for multi-hand 3D reconstruction from a still image. To the best of our knowledge, we are the first to detect and recover the textured 3D hand mesh simultaneously from images in the wild.

(2) We design a tight training scheme to optimize the overall framework in a purely weakly-supervised manner. Besides, we propose a multi-hand data augmentation strategy to verify the effectiveness of our method.

(3) Our framework supports end-to-end training and has clear advantages over previous similar methods in terms of accuracy and inference speed. Besides, our single-stage framework requires no additional third-party detectors, making it easier to deploy.

(4) Both quantitative and qualitative results demonstrate the effectiveness of our proposed framework. Our method achieves the state-of-the-art performance under the weakly-supervised setting, which even outperforms several fully-supervised model-based methods.

2. Related Work

2.1. 3D Single Hand Reconstruction.

Compared to 2D hand pose estimation that only needs to estimate 2D keypoints, 3D hand pose and mesh estimation are more challenging. Specifically, 3D hand pose estimation (Simon et al., 2017; Krejov et al., 2017; Spurr et al., 2020) only recovers the sparse hand joints while 3D hand mesh reconstruction (Zhang et al., 2019; Choi et al., 2020; Chen et al., 2021a) predicts the dense hand mesh with the richer information of hand pose and shape. In this work, we mainly focus on recovering hand mesh from single color image, which is more challenging than the depth image-based methods (Mueller et al., 2019). Generally, previous studies in this field can be roughly categorized into two groups, including model-based methods

for parameter regression and vertex-based approaches for mesh coordinates estimation.

As for model-based methods, (Boukhayma et al., 2019) directly regress shape, pose and view parameters of hand model MANO (Romero et al., 2017) and supervise with 2D and 3D joints. (Zhang et al., 2019) adopt a similar framework architecture and add the silhouette information as supervision by a differentiable render (Kato et al., 2018). To tackle the problem of lacking 3D annotated real images, (Zimmermann et al., 2019) capture a large single hand dataset with multi-view setup and obtain annotations through an iterative model fitting process. (Hampali et al., 2020) propose a similar 3D annotation method that focus on hand and object interactions. (Qian et al., 2020) present the parametric texture model of hands, and combine it with MANO parameters. (Lv et al., 2021) propose a tailor module to improve the coarsely reconstructed mesh model provided by the hand module. Recently, (Zhang et al., 2021) design a cascaded multitask learning backbone to estimate 2D hand pose, mask and mesh simultaneously, which achieves the promising single hand reconstruction performance. For vertex-based methods, (Moon and Lee, 2020) propose an image-to-lixel prediction network for 3D mesh estimation, which employ the lixel-based 1D heatmap to localize dense mesh vertex position. (Ge et al., 2019) propose a GCN-based method trained on synthetic dataset and fine-tune on real dataset with the rendered depth map as supervision. Similarly, (Choi et al., 2020) directly regress 3D coordinates using GCN but require 2D human pose as input. (Chen et al., 2021a) extend the GCN-based pipeline with a feature aggregation and 2D-1D registration for pose recovery. Recently, (Spurr et al., 2021) adopt contrastive learning to take advantage of unlabeled data to improve performance.

2.2. 3D Multi-hand Estimation

There are a few existing methods that try to address the 3D multi-hand pose estimation task. (Mueller et al., 2019) track two hands in real-time using the extra depth sensor. (Simon et al., 2017) propose the first 3D markerless hand motion capture system with multi-view setups. (Zimmermann and Brox, 2017) first predict 2D keypoints from color image for both hand and lift them to 3D pose. However, the training images are synthesized from 3D models of humans with the corresponding animations, which are far from realistic. (Panteleris et al., 2018) address this problem in real-world dataset through a three-step pipeline, namely hand area detection, key-points localization and 3D pose estimation. However, several off-the-shelf detectors (Redmon and Farhadi, 2017; Simon et al., 2017) are required in each step. (Rong et al., 2021) consider the whole-body capture problem through a standard two-stage pipeline. It firstly detects the body region, and then regresses the human and hand model parameters. Recently, there are some progress (Moon et al., 2020; Li et al., 2022) in interacting hand pose estimation. However, bounding boxes of hand area are required for inference. Most of the these methods separately detect and reconstruct multiple hands, which are computational redundant. To this end, we propose a one-stage framework for multi-hand pose estimation.

2.3. Weakly-supervised Methods

In order to get rid of the dependency on massive expensive 3D annotations, some work in recent years tries to estimate 3D hand pose with weak supervision. (Neverova et al., 2017) take the depth image as input and fuse it with a novel intermediate representation. (Cai et al., 2018) and (Wan et al., 2019) adopt a similar pipeline that initializes the network on fully-annotated synthetic data and fine-tunes it on real-world images with depth regularization. (Spurr et al., 2020) introduce a series of biomechanically inspired constraints to guide the hand prediction, including joint skeleton structure, root bone structure and joint angles. (Chen et al., 2021b) employ an off-the-shelf 2D pose detector (Simon et al., 2017) as a weaker 2D supervision, compared to human annotated 2D keypoints. Differently from the above weakly-supervised methods, our model is designed for multi-hand reconstruction from single image without bounding box.

3. Methodology

In this section, we present our proposed single-stage multi-hand reconstruction framework. Firstly, we suggest a single-stage pipeline to locate and recover multiple hands simultaneously. Then, we present the localization and reconstruction module, respectively. Finally, a global-local feature consistency loss and multi-hand data augmentation strategy are designed to boost the robustness and accuracy of our proposed approach.

3.1. Overview

The overall framework of our method is depicted in Fig. 2, which shares a classical encoder-decoder structure. Given an input image, our model recovers the position as well as 3D pose and shape of each hand in the image. Existing methods (Zimmermann and Brox, 2017; Moon et al., 2020) address this task by sequentially detecting and reconstructing 3D hand mesh in a multi-stage manner, which incurs extra computational cost on preprocessing hand area and feature extraction. The usage of additional detectors makes such methods not end-to-end. As for our proposed framework, each hand instance is localized and recovered jointly within a single forward pass. To this end, we adopt ResNet-50 (He et al., 2016) as the backbone of our encoder to extract features, where the parametric hand model MANO (Romero et al., 2017) is used as the decoder for hand mesh reconstruction. An optional branch for 2D joint heatmaps estimation is designed to boost the overall performance. Our model predicts the center location, left-right hand type, MANO parameters and rendering parameters, simultaneously.

Our overall training objective function consists of hand localization loss $\mathcal{L}_{loc}$, reconstruction loss $\mathcal{L}_{rec}$ and global-local consistency loss $\mathcal{L}_{con}$ as follows,

$$\mathcal{L} = \mathcal{L}_{loc} + \mathcal{L}_{rec} + \mathcal{L}_{con}. \tag{1}$$

The localization loss acts as a hand detector in image space. Hand center, keypoints and type are determined by local image feature. The reconstruction loss plays an important role in 3D recovery. Hand pose, shape as well as texture are regressed
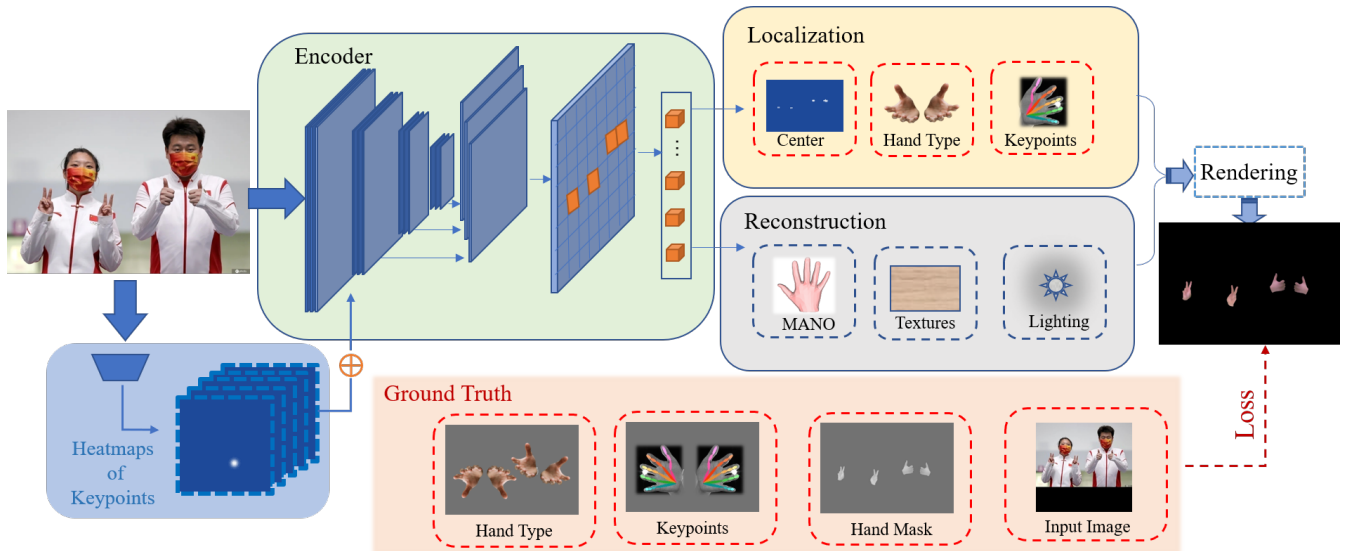
Fig. 2: Overview of the proposed framework. Given an image, we adopt ResNet as backbone to estimate heatmaps of keypoints and concatenate it with the feature map of the first layer. Encoder part encodes the input features into a center map. Each cell in the map denotes a parametric hand at that position. The localization module is responsible for decoding the hand center, left/right hand type and keypoints and the reconstruction module is responsible for predicting the 3D mesh with MANO, lighting and texture parameters. Each hand mesh is rendered into image space using PyTorch3D (Ravi et al., 2020). The whole pipeline can be supervised with only 2D labels, which is trained in an end-to-end manner.

through global feature sampled from the center map. The consistency loss ensures that the directly estimated and re-projected keypoints are consistent. We describe each module in the following.

3.2. Multiple Hand Localization

In this section, we address the problem of hand localization in a 2D image. The input image with resolution of $W \times H$ is divided into $\frac{W}{8} \times \frac{H}{8}$ cells, where each cell represents an individual hand centered in this position. Instead of directly regressing 2D keypoints to estimate hand pose like the conventional method, we predict the center location and left-right hand types to facilitate the subsequent 3D reconstruction.

Deep Hand Encoder Our backbone follows the network structure design of ResNet-50 for feature extraction. As shown in Fig. 2, we concatenate the feature maps of the last three layers and unify them into the same size of $[b, 256, H/8, W/8]$ via Conv2d and ConvTranspose2d operations. After going through Conv2d, BatchNorm2d and ReLU functions, we get the final feature map. Here b refers to batch size, followed by the number of feature channels and resolution.

As shown in Fig. 2, each cell in the feature map represents an individual hand locating at the corresponding position. The output code vector δ has all the information to construct a hand, which can be decomposed into center position $\delta_{cp} \in \mathbb{R}^1$, left-right hand type $\delta_{lr} \in \mathbb{R}^2$, 2D keypoint heat-maps $\delta_{kp} \in \mathbb{R}^{21}$, MANO parameters $\delta_{mano} \in \mathbb{R}^{61}$, texture coefficient $\delta_{text} \in \mathbb{R}^{778 \times 3}$ and lighting parameters $\delta_{light} \in \mathbb{R}^{27}$. The first three items are used to locate the hand in the 2D image. Moreover, the last three items are used to construct a 3D hand mesh that is rendered into camera space.

Hand Localization In contrast to the conventional pipeline, we introduce an extra center map to estimate the location for each hand instance. To this end, we employ a heatmap $H \in \mathbb{R}^{\frac{W}{8} \times \frac{H}{8} \times 1}$ to represent the center of each hand, in which each local peak

of the probability map indicates a potential hand instance. As discussed in literature (Pfister et al., 2015), the heatmap representation is more robust against noise compared to regressing the pixel coordinate directly. Thus, the hand center coordinates $P_{ct} = \{p_i \in \mathbb{R}^2 | 1 \le i \le k\}$, where k indicates the number of visible hands, is encoded as a Gaussian distribution. The scale of hand is integrated as Gaussian radius. The calculation of radius is referred to (Duan et al., 2019). In the multi-hand setting, hand type has to be considered during training, since the MANO models of left and right hand have different initial position and articulation range. We integrate the left-right hand type into our center map, which is different from face and body reconstruction tasks.

Given the final feature map, the localization module acts as a decoder, generating the corresponding center, hand type and keypoints predictions. We employ Conv2d to map its output channels into 1(cp), 2(lr), and 21(kp), respectively. The overall loss function of hand localization $\mathcal{L}_{loc}$ consists of three components as follows:

$$\mathcal{L}_{loc} = \lambda_{cp}\mathcal{L}_{cp} + \lambda_{lr}\mathcal{L}_{lr} + \lambda_{kp}\mathcal{L}_{kp}, \quad (2)$$

where $\mathcal{L}_{cp}$ refers to the center point localization loss. $\mathcal{L}_{lr}$ denotes the left-right hand type regression loss and $\mathcal{L}_{kp}$ is keypoints detection loss. λ is a weighting coefficient to balance the magnitude of different losses. Specifically, $\mathcal{L}_{cp}$ is a modified pixel-wise two-class logistic regression with focal loss (Lin et al., 2020). The center of each hand should be categorized as positive class 'hand' while the rest area should be treated as negative class 'background'. Since there exists imbalance between two kinds of labels, we formulate $\mathcal{L}_c$ like focal loss as below:

$$\mathcal{L}_{cp} = -\frac{1}{k} \sum_{n=1}^{w \times h} (1 - p_n)^\gamma \log(p_n), \quad (3)$$

where k is the total number of hands. $p_n \in [0, 1]$ is the estimated

confidence value for positive class, and $1 - p_n$ is the probability for negative class. $w \times h$ is the overall pixel in the center map. γ is set to 2 as a hyperparameter to reduce the relative loss for well-classified examples. $\mathcal{L}_{lr}$ also adopts focal loss to solve the problem of imbalance between the positive and negative samples except that we define '0' as left hand and '1' as right hand. $\mathcal{L}_{kp}$ shares the same formulation as $\mathcal{L}_{cp}$ with more channels for all keypoints.

3.3. Multiple Hand Mesh Reconstruction

Hand Mesh Representation For hand mesh representation, we adopt a model-based method that directly regresses the MANO parameters to shape 3D hand. It has the merit of greatly reducing the search space for poses, which alleviates the difficulty in recovering 3D shape from a single still image. This enables our method to achieve good results with only weak supervision. MANO (Romero et al., 2017) provides a low-dimensional parametric model to synthesize the hand mesh, which is learned from around 1000 high-resolution 3D hand scans of 31 different persons in a wide variety of hand poses. As in (Romero et al., 2017), we represent with the hand shape $\beta \in \mathbb{R}^{10}$ and pose $\theta \in \mathbb{R}^{51}$ as follows:

$$M(\beta, \theta) = W(V_P(\beta, \theta), \theta, \mathbb{J}(\beta), \tilde{W}), \qquad (4)$$

$$V_P(\beta, \theta) = \bar{V} + \sum_{n=1}^{|\beta|} \beta_n S_n + \sum_{n=1}^{|\theta|} (\theta_n - \bar{\theta}) P_n, \qquad (5)$$

where W is the Linear Blend Skinning (LBS) function. $\mathbb{J}$ is a predefined joint regressor, and $\tilde{W}$ is blend weights. Vertices in mesh $V_P \in \mathbb{R}^{778 \times 3}$ are calculated according to shape and pose displacements of template hand mesh $\bar{V} \in \mathbb{R}^{778 \times 3}$. S_n are the principal components in a low-dimensional shape basis and P_n are pose blend shapes controlling vertices offset. $\bar{\theta}$ is the mean pose. With the joint regressor $\mathbb{J}$, we can further calculate the accurate 3D joints $J \in \mathbb{R}^{21 \times 3}$ from the position of the vertices, corresponding to 21 keypoints in image space. It is worthy of mentioning that both global hand rotation and translation are encoded in MANO parameters, which are used in the camera projection. In order to narrow the gap between reconstruction results and real-world application, we estimate the texture parameters for each hand. As in (Chen et al., 2021b), we directly regress per-vertex RGB value $\delta_{text} \in \mathbb{R}^{778 \times 3}$ of each hand mesh. Furthermore, we employ spherical harmonics (Ramamoorthi and Hanrahan, 2001) to approximate illumination changes of the scene. The estimated lighting vector $L \in \mathbb{R}^{27}$ works well in several datasets with various illumination conditions.

Camera Model Based on the above hand mesh representation, we are able to estimate 3D hand in hand-relative coordinates. Projecting each hand into camera-relative coordinate and image coordinate system is essential for the applications. Instead of assigning different camera parameters to each individual hand like conventional multi-stage pipeline, a unified and consistent camera model is more convenient and reasonable. Therefore, we use the same intrinsic matrix K for perspective projection in each dataset during training. By predicting the individual rotation and translation matrix $T = \{[R_i|t_i] \in \mathbb{R}^{3 \times 4} | 1 \le i \le k\}$, all hand meshes are transformed into a unified camera coordinate system as follows:

$$P_i^c = KT_i P_i^w$$

$$K = \begin{bmatrix} f_x & 0 & c_x \\ 0 & f_y & c_y \\ 0 & 0 & 1 \end{bmatrix}, T_i = \begin{bmatrix} r_{11} & r_{12} & r_{13} & t_1 \\ r_{21} & r_{22} & r_{23} & t_2 \\ r_{31} & r_{32} & r_{33} & t_3 \end{bmatrix}, \qquad (6)$$

where f_x, f_y are the focal length fixed as 512 in multi-hand setting, $c_x = W/2$, $c_y = H/2$ are the projection center of the image. Global rotation and translation matrices are estimated in δ_{mano} together with other joint rotations on Rodrigues vector representation. $P^c \in \mathbb{R}^3$ is the hand mesh in camera coordinate system, and $P^w \in \mathbb{R}^3$ in world coordinate system. P^w is further expanded to a homogeneous coordinate system to calculate the matrix projection. Comparing to the conventional multi-stage methods, our approach enjoys the benefits of coherent environment light and projection model, while the cropped hand patch may lose some precision of texture and scale information. Besides, the important relative position of each hand can be easily recovered in the proposed pipeline without requiring the intrinsic matrix of each hand.

Hand Mesh Reconstruction As shown in Fig. 2, the reconstruction module also acts as a decoder, which generates the corresponding MANO, texture and light parameters. We employ Conv2d to map its output channels to parameter scales. This is the same as the localization module above. Based on the estimated MANO parameters and camera model, we are able to render hand mesh into camera space. Given an input image, our model first estimates the center map which represents all visible hands in 2D space. We use max pooling operation to find the local maximums and gather hand parameters according to these indexes. 3D hand meshes $T_P \in \mathbb{R}^{778 \times 3}$ and joints $J \in \mathbb{R}^{21 \times 3}$ are determined by $\delta_{mano} \in \mathbb{R}^{61}$, which are converted to the camera coordinate system through the estimated global rotation and translation terms. Further, we adopt 2D keypoints re-projection loss and photometric loss to learn our parameters as below:

$$\mathcal{L}_{rec} = \lambda_{rep} \mathcal{L}_{rep} + \lambda_{pho} \mathcal{L}_{pho} + \lambda_{reg} \mathcal{L}_{reg}, \qquad (7)$$

where $\mathcal{L}_{rep}$ refers to the re-projection loss. $\mathcal{L}_{pho}$ is the photometric loss, and $\mathcal{L}_{reg}$ represents the regularization loss. Specifically, $\mathcal{L}_{rep}$ is the sparse 2D keypoints re-projection error that minimizes the distance between 2D projection from its corresponding 3D joints and the labelled 2D ground truth.

$$\mathcal{L}_{rep} = \frac{1}{k \times J} \sum_{n=1}^{k} \sum_{j=1}^{J} \|\phi_{n,j} - \phi_{n,j}^*\|_2$$
$$+ \frac{1}{k \times E} \sum_{n=1}^{k} \sum_{e=1}^{E} \|e_{n,e} - e_{n,e}^*\|_2 \qquad (8)$$

In $\mathcal{L}_{rep}$, J is the total number of 2D keypoints, and E is the total number of normalized edge vectors constructed based on each two adjacent keypoints. They correspond to 21 joints and 20 movable bones in the physical sense. $\phi_{n,j}$ refers to the nth hand and j^{th} keypoint projected on image. $e_{n,e}$ is the nth hand and e^{th} bone. Similarly, $*$ indicates the ground truth. We use the length of the first section in the middle finger to unify the errors for different hand scales.

$$\mathcal{L}_{pho} = \frac{\sum_{n=1}^{W \times H} M_n \|I_n - I_n^*\|_2}{\sum_{n=1}^{W \times H} M_n}. \qquad (9)$$

$\mathcal{L}_{pho}$ is the photometric error between the input and rendered images. Hand mask is used to exclude the influence of irrelevant background pixels. I and I^* are the rendered and input images, respectively. M is a binary mask with the same size of input image, which is determined by Hadamard product between the rendered silhouette and ground truth skin mask. Since we ignore the pixels in background area, M_n in such positions is just set to zero. 3D textured hand mesh is constructed with δ_{mano}, δ_{text} and δ_{light} and the rendering is implemented through PyTorch3D (Ravi et al., 2020).

$\mathcal{L}_{reg}$ is a pose and shape regularization term to penalize the implausible 3D joint rotation and shape. We define an interval $[\theta_{min}, \theta_{max}]$ of valid rotation range for each joint angle, since the angle within the range should not be regularized. Shape parameters are encouraged to be close to the mean value. In this paper, we define the regularization loss as below:

$$\mathcal{L}_{reg} = w_{pose}\|\delta_{pose}\|_1 + w_{shape}\|\delta_{shape}\|_2, \qquad (10)$$

where δ_{pose} is the pose error that penalizes θ exceeding the predefined threshold, and δ_{shape} is the shape error pulling β to be close to mean shape.

Global-local Feature Consistency To further improve the performance, we consider combining the global feature and local feature together. Specifically, the 2D keypoints directly estimated from local features and re-projected points from 3D joints estimated from global features should be equal. Interestingly, our center map plays an important role in top-down estimation while our 2D keypoints heatmap is essential to bottom-up estimation.

$$\mathcal{L}_{con} = \frac{1}{k \times J} \sum_{n=1}^{k} \sum_{j=1}^{J} \|\phi_{n,j}^{kp} - \phi_{n,j}^{rep}\|_2. \qquad (11)$$

Similar ideas have been addressed in single-hand methods as intermediate supervision. In multi-hand issue, however, we have to consider the joint assignment task. Keypoints belong to the same hand should be close to each other while different hands should fall apart from each other. We use L2 normal to constrain the above assumptions.

3.4. Weakly-supervised Data Augmentation

To address the problem of lacking annotated training data with multiple hands, we synthesize a large multiscale multi-hand dataset, whose hand samples are selected from the existing single hand datasets, as shown in Fig. 7. This dataset is mainly used to verify the correctness of our method, and can also be used as pre-training data for other multi-hand methods. Specifically, we crop up to 10 hand samples and resize them to paste on an empty image $I \in \mathbb{R}^{512 \times 512}$. To generate more photo-realistic image, we firstly paste one whole image containing single hand and background, which is resized to I and padded with background pixels. Then, we crop other hand

samples according to its bounding box and randomly re-scale them into the size between 96 pixels to 320 pixels. For simplicity, we crop each hand in the original image into a square. The irrelevant background pixels are removed by hand masks. To place the hand samples, we use the greedy strategy to set them layer by layer from the lower right corner to the upper left corner in the image. The size of the next sample is randomly generated according to the remaining available space until the rest available space is less than the predefined minimum sample size. As for ground truth construction, we retain the index of each hand sample, 2D keypoints, center point, bounding box and mask, which are generated from the original data labels by affine transformation. Besides, we randomly flip the original hand patch horizontally to construct a left-hand image for hand type learning, since all images in FreiHAND and HO3D only have right hands.

4. Experiment

In this section, we thoroughly evaluate our proposed framework. Firstly, we present the implementation details for experimental setup. Then, the comprehensive experiments are conducted in order to compare with the state-of-the-art methods, including single-hand setting, two-hand setting and multi-hand setting. Finally, we give an ablation study to examine the effect of each individual module and give the potential direction for further improvement.

4.1. Implementation Details

The proposed framework is implemented with PyTorch (Paszke et al., 2019). Our method can simultaneously train detection and reconstruction modules in end-to-end. To facilitate exploring the impact of different modules on model performance, we also design a staged training strategy. In the first stage, we reduce the model task to single hand reconstruction and only update the reconstruction parameters. In the second stage, we perform joint training of detection and reconstruction based on the model obtained in the previous stage. In our training process, the batch size is set to 256, and the initial learning rate is 10^{-3}. We decrease our learning rate by 10 at the epoch of 30, 90 and 120. We train our model with four RTX2080Ti GPUs, which takes around a day to train 70K iterations on FreiHAND dataset. The input images are resized into 224×224 for single-hand estimation task and 512×512 for multiple hand recovering task. The typical data augmentation methods, including random scaling, translation, rotation and color jittering, are performed in both single and multiple hand settings.

4.2. Datasets and Evaluation Metrics

FreiHAND (Zimmermann et al., 2019) is a large-scale single hand dataset with 3D labels on hand joints and MANO parameters. The evaluation set contains 3960 samples without ground truth annotations. Researchers need to submit their predictions to the online server for evaluation. The training set contains 32,560 samples of real human hands captured with green screen

Table 1: Comparison with state-of-the-art model-based

methods on the FreiHAND dataset. Bold represents the best result and underlined represents the second-best result.

Methods	supervision	camera intrinsic	MPJPE↓	AUC_J↑	MPVPE↓	AUC_V↑	F_5↑	F_{15}↑
Boukhayma et al. (Boukhayma et al., 2019)	3D	Yes	3.50	0.351	1.32	0.738	0.427	0.895
ObMan (Hasson et al., 2019)	3D	Yes	1.33	0.737	1.33	0.736	0.429	0.907
ManoCNN (Zimmermann et al., 2019)	3D	Yes	1.10	0.783	1.09	0.783	0.516	0.934
ManoFit (Zimmermann et al., 2019)	3D	Yes	1.37	0.730	1.37	0.729	0.439	0.892
HTML (Qian et al., 2020)	3D	Yes	1.11	0.781	1.10	0.781	0.508	0.930
HIU(single) (Zhang et al., 2021)	3D	Yes	0.89	0.824	0.92	0.819	0.571	0.961
HIU(cascaded) (Zhang et al., 2021)	3D	Yes	**0.71**	**0.860**	**0.73**	**0.856**	**0.699**	**0.974**
HandTailor (Lv et al., 2021)	3D	Yes	0.82	-	0.87	-	-	-
Ours	3D	No	<u>0.80</u>	<u>0.840</u>	<u>0.81</u>	<u>0.839</u>	<u>0.649</u>	<u>0.966</u>
Biomechanical (Spurr et al., 2020)	2D	Yes	1.13	0.780	-	-	-	-
S2HAND (Chen et al., 2021b)	2D	Yes	1.18	0.766	1.19	0.765	0.48	0.92
Ours	2D	No	**1.07**	**0.788**	**1.10**	**0.782**	**0.500**	**0.937**

Table 2: Comparison with previous model-based methods on HO-3D evaluation dataset.

Methods	supervision	MPJPE↓	AUC_J↑	MPVPE↓	AUC_V↑	F_5↑	F_{15}↑
HO3D (Hampali et al., 2020)	3D	1.07	0.788	1.06	0.790	0.51	0.94
ObMan (Hasson et al., 2019)	3D	-	-	1.10	0.780	0.46	0.93
Photometric (Hasson et al., 2020)	3D	1.11	0.773	1.14	0.773	0.43	0.93
Ours	3D	**1.01**	**0.799**	**0.97**	**0.805**	**0.524**	**0.953**
PeCLR (Spurr et al., 2021)	2.5D	1.09	0.78	-	-	-	-
S2HAND (Chen et al., 2021b)	2D	1.14	0.773	1.12	0.777	0.45	0.93
Ours	2D	**1.03**	**0.794**	**1.01**	**0.797**	**0.502**	**0.951**

Table 3: EPE comparison on RHD dataset. GT S and GT H denote ground truth scale and hand type (left/right), respectively. y means ground truth used during inference while n means not used.

Methods	GT S	GT H	EPE↓
RHD (Zimmermann and Brox, 2017)	y	y	3.04
yang2019disentangling (Yang and Yao, 2019)	y	y	1.99
spurr2018cross (Spurr et al., 2018)	y	y	**1.97**
spurr2018cross (Spurr et al., 2018)	n	n	2.25
InterNet (Moon et al., 2020)	n	n	2.08
Ours	n	n	**2.07**

background, and each sample is augmented with different synthetic backgrounds. The whole dataset contains 130,240 images with various hand poses and augmented background using different post-processing options.

HO-3Dv2 (Hampali et al., 2020) is a single hand dataset with 3D annotations similar to FreiHAND, which focuses on hand-object pose estimation. It contains 68 sequences captured with 10 different persons manipulating 10 different objects. The training set has 66,034 images (from 55 sequences) and the evaluation set contains 11,524 images (from 13 sequences).

RHD (Zimmermann and Brox, 2017) is a large-scale synthetic dataset with 3D annotations for single and interacting hand poses. It is created from 3D models of humans animations using commercial software. The dataset is built upon 20 different characters performing 39 actions, providing 41,258 images for training and 2728 images for evaluation.

InterHand2.6M (Moon et al., 2020) is a large-scale real-world

dataset with 3D annotations for interacting hand poses. It contains 1,179,648 interacting hand frames and 1,410,699 single hand frames.

Evaluation Metrics As in (Zimmermann et al., 2019; Hampali et al., 2020), we evaluate our approach by calculating the errors of 3D joints and 3D vertices. We compute the mean per joint position error (MPJPE) and mean per vertex position error (MPVPE) between the prediction and ground truth in cm for 3D joints and 3D mesh evaluation, respectively. All results on Frei-HAND and HO-3D are submitted to online server that aligned automatically based on Procrustes analysis (Gower, 1975) for fair comparison. We also calculate the area under curve (AUC_J for joints and AUC_V for vertices) of the percentage of correct keypoints (PCK) curve in an interval from 0 cm to 5 cm with the 100 equally spaced thresholds. Besides, end point error (EPE) is used in two-hand setting, which is defined as a mean Euclidean distance (cm) between the predicted 3D hand pose and ground-truth after root joint alignment. As for 2D keypoint evaluation, we calculate MPJPE using 2D distance in *pixel*.

4.3. Comparisons with State-of-the-art Methods

Single-hand Reconstruction Experiments We firstly compare our method against the recent state-of-the-art methods in fully-supervised (Boukhayma et al., 2019; Zimmermann et al., 2019; Hasson et al., 2019; Qian et al., 2020; Hasson et al., 2020; Hampali et al., 2020; Zhang et al., 2021; Spurr et al., 2021) and weakly-supervised manner (Spurr et al., 2020; Chen et al., 2021b). For fair comparison, we mainly focus on the more relevant model-based methods and some excellent We choose Frei-

(a)   (b)
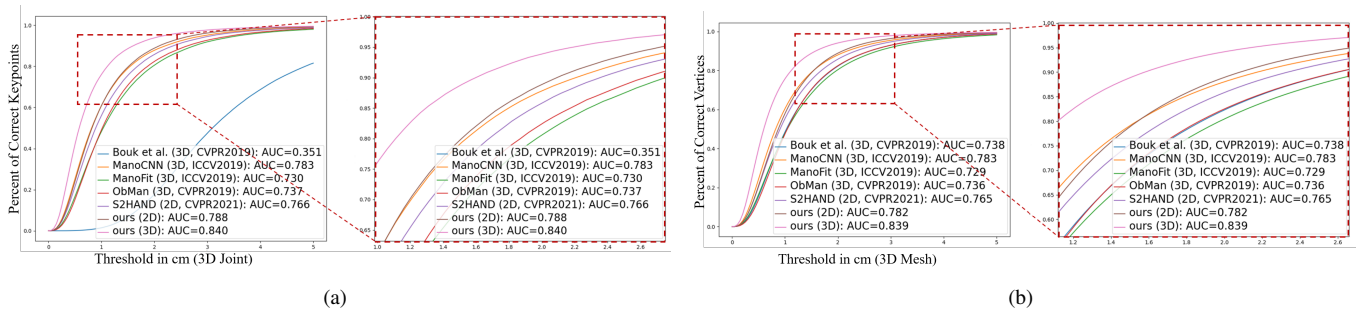
Fig. 3: 3D PCK comparison with state-of-the-art methods on FreiHAND dataset. The left two figures show the result of AUC_J and locally enlarged details. The right two figures show the result of AUC_V as well as locally enlarged details.

(a) Input Image (b) Ground Truth (c) Prediction (d) Viewpoint A (e) Viewpoint B   (f) Input Image (g) Ground Truth (h) Prediction (i) Viewpoint A (j) Viewpoint B
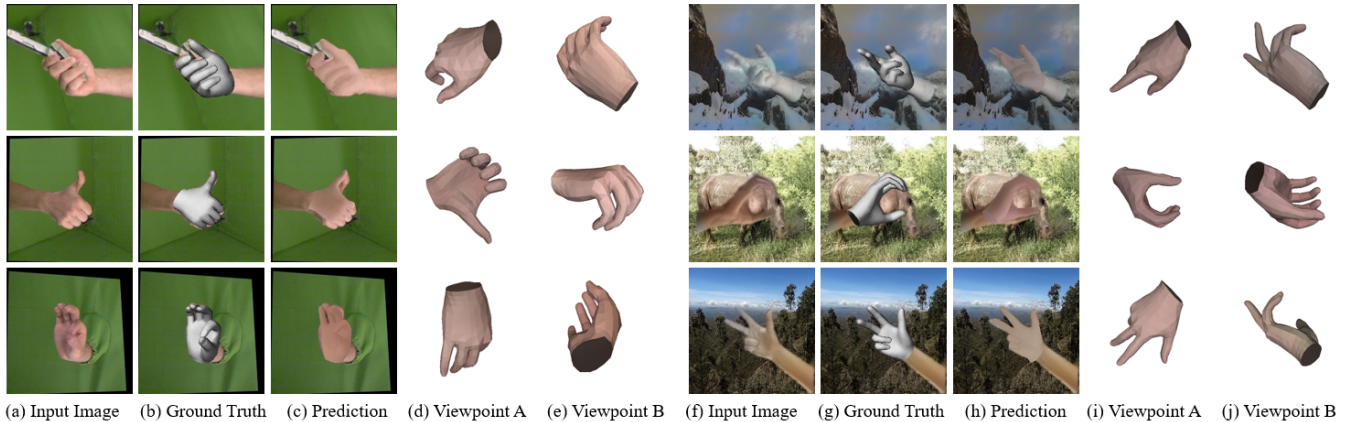
Fig. 4: Qualitative mesh results on dataset FreiHAND. Our model is trained only with 2D supervision, which do not require the real camera intrinsic parameters. Textures are learned through a self-supervised manner, which makes our outputs more vivid.

HAND and HO-3D as our validation datasets, since they are the latest and mostly used single hand datasets. Evaluations are conducted through submitting our estimated results to their online judging system[1], [2].

Table 1 shows the evaluation results on FreiHAND. It can be clearly seen that our presented method outperforms other weakly-supervised methods on all evaluation metrics, which achieves the comparable accuracy against many recent fully-supervised methods. It obtains 1.07 cm MPJPE with 0.787 AUC_J and 1.10 cm MPVPE with 0.782 AUC_V. To further explore the potential of our model, we trained it with full supervision when 3D labels are available. Our model also achieves state-of-the-art performance among model-based methods. Note that the HIU (cascaded) in Table 1 employs up to 8 cascaded networks following a coarse-to-fine design while our model only uses a single encoder. For fair comparison, we also report the results of HIU (single) from its ablation experiments, using the same single encoder-decoder structure as ours. Our method performs better while having the same model complexity. This reflects the potential of our framework. Fig. 3 plots our 3D PCK of joints and vertices with other methods under different error thresholds. Our fully-supervised model outperforms other methods to a large margin, while our weakly-supervised model achieves the comparable performance against

ManoCNN (Zimmermann et al., 2019). In the close-up figure, it can be found that our weakly-supervised model is not as good as ManoCNN under the small error thresholds while our method performs better under the large thresholds. This is because it is hard for our method to learn the detailed 3D pose with only 2D label. However, we can achieve generally consistent and fine-grained accuracy. To evaluate 2D pixel error, we randomly select 10% of the training set for validation, since no ground-truth 2D keypoints available on evaluation set. We train our model with the rest samples of the training set, which obtains 6.64 pixel error/1.29 cm joint absolute error under the input size of 224×224 using 2D supervision. Moreover, we obtain 5.88 pixel error/0.65 cm joint absolute error with 3D supervision. The close pixel error further demonstrates that our presented method can fully make use of 2D supervision to learn the accurate 3D poses, while 3D supervision can disambiguate the perspective projection to further improve performance. Visual results on validation set are depicted in Fig. 4, which include the input image, ground-truth mesh overlaid on input image, predicted mesh overlaid on input image and textured mesh in two viewpoints. By taking advantage of the photometric loss, our model is able to learn the lighting and texture parameters from input image through a self-supervised manner, which produces more vivid hand mesh. As shown in Fig. 4, two sets of images from different viewpoints were rendered using open-source system MeshLab (Cignoni et al., 2008) without lighting.

HO3D is a more challenging dataset for the hand-object interaction containing motion sequences. Hands are usually

---

[1] https://competitions.codalab.org/competitions/21238

[2] https://competitions.codalab.org/competitions/22485

occluded by the object or partly outside the screen, which makes it even more challenging for our presented method to estimate the hand center. By making use of the center-based pipeline and carefully designed constraints, our approach achieves the very promising performance in both weakly-supervised and fully-supervised settings. As shown in Table 2, our weakly-supervised model outperforms all other model-based methods while our fully-supervised method further improves the performance. We show the visual results of our method and the current state-of-the-art weakly-supervised method S2HAND (Chen et al., 2021b) in Fig. 5. It can be seen that our method has obvious advantages in both texture detail and pose estimation.

(a) Input Image   (b) S2HAND   (c) Ours
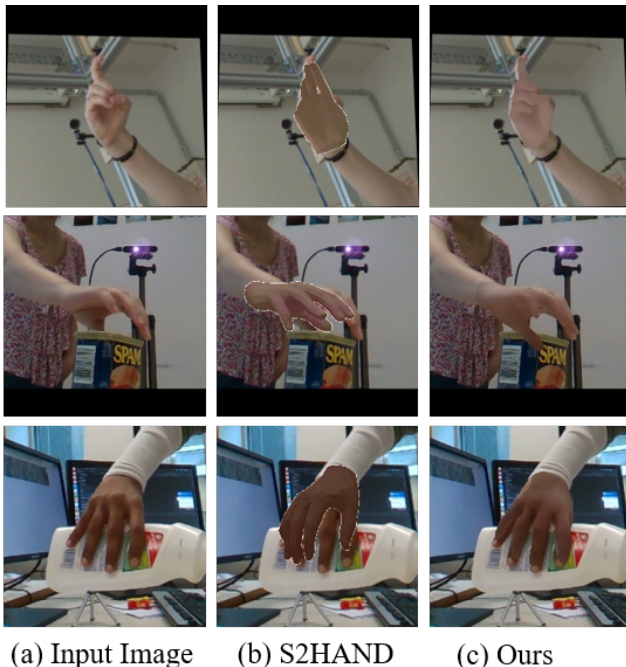
Fig. 5: Visualization comparison with the state-of-the-art method on single hand datasets. Our method achieves significant advantages in both hand pose accuracy and texture realism.

Table 4: Performance comparison with multi-stage methods on multi-hand datasets. We compare the results of our multi-hand model and S2HAND (Chen et al., 2021b) equipped with a third-party detector (Shan et al., 2020), and the results of S2HAND directly using ground-truth bounding boxes, evaluating 2D keypoint distances (pixels) and 3D joint point errors (cm).

Methods	S2HAND +Detector	Ours_Multi	S2HAND+GT
2D Distance↓	9.79	**7.41**	9.54
MPJPE↓	1.55	**0.95**	1.52

Two-hand Reconstruction Experiments Secondly, we evaluate our method on RHD and InterHand2.6M with two isolated hands and interacting hand scenarios, respectively.

As for RHD, we compare our method with several fully-supervised methods (Zimmermann and Brox, 2017; Yang and Yao, 2019; Spurr et al., 2018; Moon et al., 2020), where the EPE results in Table 3 are reported from (Moon et al., 2020). All of the above methods only predict the sparse hand joints rather than dense hand mesh, they require the ground truth bounding
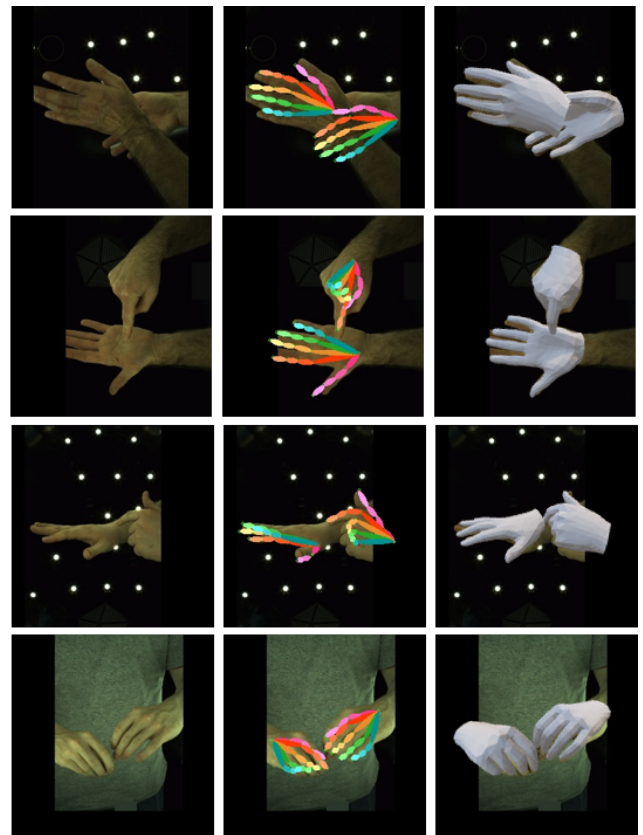
(a) Input Image   (b) Keypoints   (c) Mesh

Fig. 6: Qualitative 3D pose estimation results on InterHand2.6M dataset.

box to crop the hand areas. To facilitate the fair comparisons, we train our model with the same cropped images and evaluate the relative 3D joints error. It can be seen that our weakly-supervised model achieves the promising result without requiring 3D supervision, ground truth scale or hand type. We obtain 2.07 cm end point error for 3D joints and 8.09 pixel error under input resolution of 224×224. Differently from single-hand setting, it is challenging to distinguish between left and right hand types while recovering 3D pose. We achieve 97.65% accuracy for hand type classification. As a single stage pipeline, we can detect and recover hands, simultaneously. Furthermore, we train our model using the original image, which achieve the 2.10 cm end point error for 3D joints and 9.14 pixel error under input resolution of 320×320. The tiny accuracy loss demonstrates the effectiveness of our proposed single-stage pipeline.

To examine the performance of our presented method on images captured in the real world, we select 200K images from the training set of InterHand2.6M to train the model and use the whole testing set for evaluation. It spends lots of computational cost on training all the data together. Similar to RHD, we firstly train our model with the cropped images and evaluate the relative 3D joints error. We achieve 2.77 cm end point error and 10.98pixel error under the input size of 224×224. Then, we train our model using the original image without cropping. It achieves 2.39 cm end point error for 3D joints and 15.82 pixel error under input resolution of 512×512. Due to the difference between our fixed focal length in training and the ground truth, the predicted 3D coordinates and the true value from the

dataset cannot be completely matched. Therefore, the 2D loss in this experiment can more accurately reflect the performance of our presented method. Visualization results are shown in Fig. 6. In further work, we consider processing a group of two interacting hands together like InterHand (Moon et al., 2020) or introduce other assumptions such as collision detection and left-right hand association to improve the accuracy.

Table 5: Comparison on different combinations of loss terms tested on the evaluation set of FreiHAND. Each loss term can improve the performance of the model to a certain extent, and the photometric loss mainly predicts texture and lighting to restore realistic meshes.

Baseline	$\mathcal{L}_{reg}$	$\mathcal{L}_{aug}$	$\mathcal{L}_{con}$	$\mathcal{L}_{bone}$	$\mathcal{L}_{pho}$	$\mathcal{L}_{3D}$	MPJPE↓	MPVPE↓
✓	-	-	-	-	-	-	2.98	3.16
✓	✓	-	-	-	-	-	1.66	1.72
✓	✓	✓	-	-	-	-	1.53	1.61
✓	✓	-	✓	-	-	-	1.64	1.71
✓	✓	-	✓	✓	-	-	1.43	1.45
✓	✓	✓	✓	-	-	-	1.48	1.56
✓	✓	✓	-	✓	-	-	1.13	1.17
✓	✓	✓	✓	✓	-	-	1.07	1.10
✓	✓	✓	✓	✓	✓	-	**1.07**	**1.10**[*]
✓	✓	✓	✓	✓	-	✓	0.80	0.81
✓	✓	✓	✓	✓	✓	✓	**0.80**	**0.81**[*]

[*] this is the dense mesh with vivid hand texture.

Table 6: PSNR comparison of reconstruction results tested on evaluation set of FreiHAND and HO3D. Ours_mean denotes our model using mean texture.

Dataset	FreiHAND↑	HO3D↑
S2HAND (Chen et al., 2021b)	14.74	13.92
Ours_mean	11.79	13.71
Ours	**16.64**	**16.78**

Multi-hand Reconstruction Experiments To verify the effectiveness of our method in multi-handed scenarios, we use the data augmentation strategy proposed above to generate a new validation dataset for experiments. Since there are few off-the-shelf methods that can handle the multi-hand reconstruction, we solve it by equipping the existing single-hand reconstruction method with an extra detector. We choose S2HAND (Chen et al., 2021b) for comparison, since it adopts a similar model-based approach and provides training code as well as evaluating models. We employ EgoHand (Shan et al., 2020) as the detector. It is specially trained from an egocentric perspective that is close to the multi-hand data we want to test on. We compare the 2D pixel error and MPJPE of our multi-hand model with the detector-equipped S2HAND. To examine the influence of the detector on the reconstruction accuracy, we test the results of directly utilizing the ground-truth hand bounding box as input. As shown in Table 4, our method achieves clear advantages in both cases. Fig. 7 depicts the visual results of our multi-hand model, including input image, the predicted mask, keypoints and mesh overlaid with the input image, respectively. In order to investigate the generalization ability of our proposed approach, we evaluate our model on the unlabeled images from Bambach et al. (Bambach et al., 2015). As shown in Fig. 8, our method can obtain the reasonable prediction results even without fine-tuning. To achieve better accuracy in real scenes, the model can be fine-tuned using manually annotated 2D key-

points in the target scene, since 2D labels are easier to obtain than 3D labels.

(a) Input Image　(b) Mask　(c) Keypoints　(d) Mesh
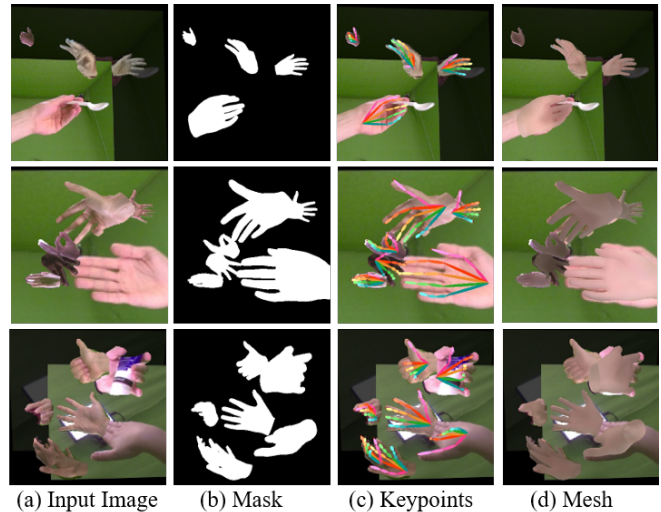
Fig. 7: Qualitative 3D pose estimation results on the proposed multi-hand dataset. From left to right: generated image, predicted mask, predicted keypoints and predicted mesh overlaid on input image.

Fig. 8: Qualitative 3D pose estimation results on images in the wild. The predicted keypoints are re-projected from estimated 3D mesh using our model, which is trained only on our generated multi-hand data.

4.4. Ablation Study

Evaluation on Efficiency The conventional methods using multi-stage pipeline need to detect and encode each hand patch individually while our presented network shares the same feature map only requiring single forward pass for inference. For the single-hand setting, we employ the input image with the size of 224×224. To facilitate the fair comparison, we conduct the experiments on the same device, and use the official implementation of the reference methods. Our model only takes 11.8ms for inference, while S2HAND (Chen et al., 2021b) spends 58.7ms and InterHand (Moon et al., 2020) requires 16.4ms with the same input. It can be seen that our model is the most lightweight under the same conditions. As for the multi-hand setting, the computation cost of multi-stage methods grows linearly with the number of hands in image, as depicted in Fig. 9. In addition, detection and cropping time need to be considered, which incurs the extra computation cost and requires off-the-shelf detectors. Besides, we find that the running time of our model mainly depends on the size of input image. The inference time with the size of 512×512 is 36.5ms, which is still faster than S2HAND. Through this experiment, we believe that

the single-stage framework we proposed has its merit in dealing with multiple hands.
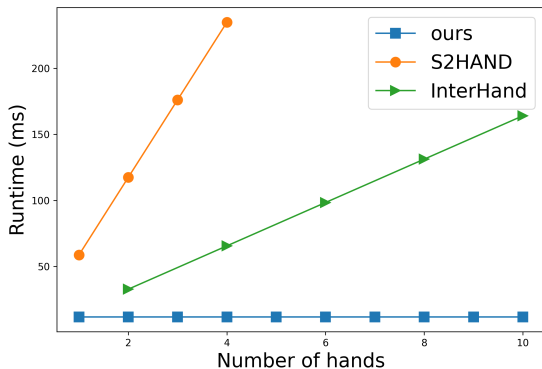
Fig. 9: Runtime comparison on the different number of hands. The computational cost grows linearly using a multi-stage pipeline, while our single-stage pipeline only needs a single forward pass.

Hand Center We study several center definitions such as the center of bounding box, mean position of visible landmarks and fixed joint position like wrist or first part of middle finger. Firstly, the fixed joint position is unsuitable for all kinds of datasets. In some datasets, the invisible joints are set to -1, which makes this definition not applicable when the fixed center location is invisible. Then, we test the accuracy of center definition on FreiHAND using the center of bounding box and mean position of visible landmarks. The former achieves 1.09 cm MPJPE and 1.12 cm MPVPE while the latter obtains 1.07 cm MPJPE and 1.10 cm MPVPE. In some poses, the center of the bounding box may fall on background pixels outside the hand, while the center of the mean position of visible landmarks can mostly fall on the area belonging to the hand. Therefore, we choose the latter for its robustness.

Effect of Different Loss Terms Finally, we conduct a comprehensive comparison on different loss terms. The overall comparison results on FreiHAND dataset are depicted in Table 5. The re-projected keypoints error is the most fundamental loss function for our weakly-supervised pipeline, which is treated as a baseline. $\mathcal{L}_{bone}$ is the second term in $\mathcal{L}_{rep}$ that introduces constraint on 2D bone direction. It provides more detailed pose information, which plays an import role in our weakly-supervised algorithm. $\mathcal{L}_{cons}$ introduces the top-down and bottom-up consistency, which further improves the overall accuracy. $\mathcal{L}_{pho}$ does little improvement for pose accuracy, since other losses have been able to constrain the optimization direction of the model. However, the results without $\mathcal{L}_{pho}$ are with purely gray texture. Compared to S2HAND, our method achieves higher PSNR (Peak Signal to Noise Ratio) scores, which means our predictions are more realistic, as shown in Fig. 5. Detailed PSNR results can be found in Table 6. $\mathcal{L}_{reg}$ is adopted to avoid the implausible 3D poses, which makes the limited contribution to the final accuracy. In some cases, it even reduces the accuracy. However, a lower loss with the unreasonable hand shape is not the expected result, which often means overfitting. The difference between with and without $\mathcal{L}_{reg}$ is depicted in Fig. 10. Besides, $\mathcal{L}_{aug}$ is not a specific loss term, which refers to whether

to use the data augmentation strategy mentioned above during training. The data augmentation can significantly improve the model accuracy, which can avoid overfitting and make full use of the underlying pose distribution. $\mathcal{L}_{3D}$ refers to the extra joint constraints when 3D supervision exists. The loss term is the same as $\mathcal{L}_{cons}$ except that the constrained objects are 3D joints.

| (a) Input Image | (b) w/o $\mathcal{L}_{reg}$ | (c) w/ $\mathcal{L}_{reg}$ | (d) Input Image | (e) w/o $\mathcal{L}_{reg}$ | (f) w/ $\mathcal{L}_{reg}$ |
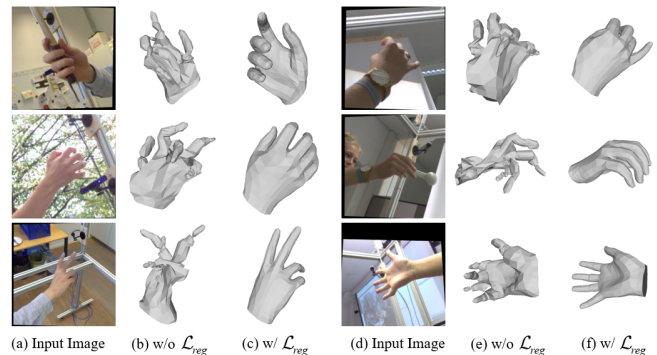
Fig. 10: Visual comparison of model trained with and without pose regularization term $\mathcal{L}_{reg}$. Models without pose regularization constraints may generate implausible hand poses.
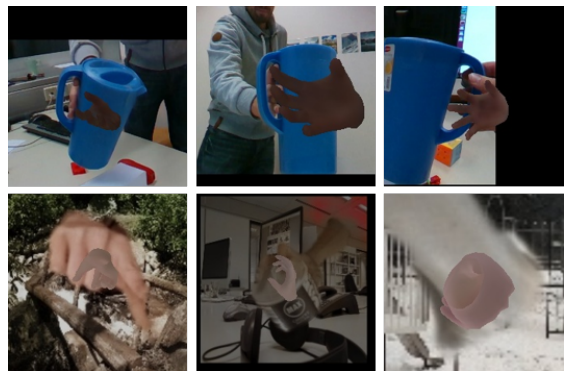
Fig. 11: Failure cases, including extreme hand pose and texture.

Limitations With only 2D supervision, it is difficult for our model to handle the ambiguity of some specific gestures. Specifically, two gestures that are symmetrical with respect to the projection plane are identical in the 2D projection view. Additionally, it is difficult for our model to get the accurate result when the input gesture is too challenging. Fig. 11 shows some failure cases, including object occlusion, motion blur, extreme texture and lighting.

5. Conclusion

This paper proposed a novel approach to simultaneously locating and recovering multiple hands from single 2D images. In contrast to the conventional methods, we presented a concise but efficient single-stage pipeline that reduced the computational redundancy in data preprocessing and feature extraction. Specifically, we designed a multi-head auto-encoder structure for multi-hand recovery, where each head network shares the same feature map and outputs hand center, pose and texture, respectively. Besides, a weakly-supervised scheme was proposed to alleviate the burden of expensive 3D real-world data annotations. Extensive experiments on the bench-

mark datasets demonstrate the efficacy of our proposed framework. Our method achieved the promising results comparing to the previous state-of-the-art model-based methods in both weakly-supervised and fully-supervised settings. In further work, we intend to extend our work to real-time hand gesture recognition (Michalis Lazarou, 2021) and human-scene interaction (Hassan et al., 2021) using multi-view contrastive learning and temporal consistency. It may reduce the burden of 3D annotation and achieve the high reconstruction accuracy.

References

Bambach, S., Lee, S., Crandall, D.J., Yu, C., 2015. Lending a hand: Detecting hands and recognizing activities in complex egocentric interactions, in: Proceedings of the IEEE/CVF International Conference on Computer Vision (ICCV), pp. 1949–1957.

Boukhayma, A., de Bem, R., Torr, P.H., 2019. 3d hand shape and pose from images in the wild, in: Proceedings of the IEEE/CVF Conference on Computer Vision and Pattern Recognition (CVPR), pp. 10843–10852.

Cai, Y., Ge, L., Cai, J., Yuan, J., 2018. Weakly-supervised 3d hand pose estimation from monocular rgb images, in: Proceedings of the European Conference on Computer Vision (ECCV), pp. 678–694.

Chen, X., Liu, Y., Ma, C., Chang, J., Wang, H., Chen, T., Guo, X., Wan, P., Zheng, W., 2021a. Camera-space hand mesh recovery via semantic aggregation and adaptive 2d-1d registration, in: Proceedings of the IEEE/CVF Conference on Computer Vision and Pattern Recognition (CVPR), pp. 13269–13278.

Chen, Y., Tu, Z., Kang, D., Bao, L., Zhang, Y., Zhe, X., Chen, R., Yuan, J., 2021b. Model-based 3d hand reconstruction via self-supervised learning, in: Proceedings of the IEEE/CVF Conference on Computer Vision and Pattern Recognition (CVPR), pp. 10446–10455.

Choi, H., Moon, G., Lee, K.M., 2020. Pose2mesh: Graph convolutional network for 3d human pose and mesh recovery from a 2d human pose, in: Proceedings of the European Conference on Computer Vision (ECCV), pp. 769–787.

Cignoni, P., Callieri, M., Corsini, M., Dellepiane, M., Ganovelli, F., Ranzuglia, G., 2008. Meshlab: an open-source mesh processing tool, in: Eurographics Italian Chapter Conference, pp. 129–136.

Duan, K., Bai, S., Xie, L., Qi, H., Huang, Q., Tian, Q., 2019. Centernet: Keypoint triplets for object detection, in: Proceedings of the IEEE/CVF International Conference on Computer Vision (ICCV), pp. 6568–6577.

Ge, L., Ren, Z., Li, Y., Xue, Z., Wang, Y., Cai, J., Yuan, J., 2019. 3d hand shape and pose estimation from a single rgb image, in: Proceedings of the IEEE/CVF Conference on Computer Vision and Pattern Recognition (CVPR), pp. 10833–10842.

Gower, J.C., 1975. Generalized procrustes analysis. Psychometrika 40, 33–51.

Hampali, S., Rad, M., Oberweger, M., Lepetit, V., 2020. Honnotate: A method for 3d annotation of hand and object poses, in: Proceedings of the IEEE/CVF Conference on Computer Vision and Pattern Recognition (CVPR), pp. 3193–3203.

Hassan, M., Ghosh, P., Tesch, J., Tzionas, D., Black, M.J., 2021. Populating 3d scenes by learning human-scene interaction, in: Proceedings of the IEEE/CVF Conference on Computer Vision and Pattern Recognition (CVPR), pp. 14703–14713.

Hasson, Y., Tekin, B., Bogo, F., Laptev, I., Pollefeys, M., Schmid, C., 2020. Leveraging photometric consistency over time for sparsely supervised hand-object reconstruction, in: Proceedings of the IEEE/CVF Conference on Computer Vision and Pattern Recognition (CVPR), pp. 571–580.

Hasson, Y., Varol, G., Tzionas, D., Kalevatykh, I., Black, M.J., Laptev, I., Schmid, C., 2019. Learning joint reconstruction of hands and manipulated objects, in: Proceedings of the IEEE/CVF Conference on Computer Vision and Pattern Recognition (CVPR), pp. 11799–11808.

He, K., Zhang, X., Ren, S., Sun, J., 2016. Deep residual learning for image recognition, in: Proceedings of the IEEE/CVF Conference on Computer Vision and Pattern Recognition (CVPR), pp. 770–778.

Kato, H., Ushiku, Y., Harada, T., 2018. Neural 3d mesh renderer, in: Proceedings of the IEEE/CVF Conference on Computer Vision and Pattern Recognition (CVPR), pp. 3907–3916.

Krejov, P., Gilbert, A., Bowden, R., 2017. Guided optimisation through classification and regression for hand pose estimation. Computer Vision and Image Understanding 155, 124–138.

Li, M., An, L., Zhang, H., Wu, L., Chen, F., Yu, T., Liu, Y., 2022. Interacting attention graph for single image two-hand reconstruction, in: Proceedings of the IEEE/CVF Conference on Computer Vision and Pattern Recognition (CVPR).

Lin, K., Wang, L., Liu, Z., 2021a. End-to-end human pose and mesh reconstruction with transformers, in: Proceedings of the IEEE/CVF Conference on Computer Vision and Pattern Recognition (CVPR).

Lin, K., Wang, L., Liu, Z., 2021b. Mesh graphormer. 2021 IEEE/CVF International Conference on Computer Vision (ICCV) , 12919–12928.

Lin, T.Y., Goyal, P., Girshick, R., He, K., Dollar, P., 2020. Focal loss for dense object detection. IEEE Transactions on Pattern Analysis and Machine Intelligence 42, 318–327.

Lv, J., Xu, W., Yang, L., Qian, S., Mao, C., Lu, C., 2021. Handtailor: Towards high-precision monocular 3d hand recovery, in: British Machine Vision Conference (BMVC).

Michalis Lazarou, Bo Li, T.S., 2021. A novel shape matching descriptor for real-time hand gesture recognition. Computer Vision and Image Understanding 210, 103241.

Moon, G., Lee, K.M., 2020. I2l-meshnet: Image-to-lixel prediction network for accurate 3d human pose and mesh estimation from a single RGB image, in: Proceedings of the European Conference on Computer Vision (ECCV), pp. 752–768.

Moon, G., Yu, S.I., Wen, H., Shiratori, T., Lee, K.M., 2020. Interhand2.6m: A dataset and baseline for 3d interacting hand pose estimation from a single rgb image, in: Proceedings of the European Conference on Computer Vision (ECCV).

Mueller, F., Davis, M., Bernard, F., Sotnychenko, O., Verschoor, M., Otaduy, M.A., Casas, D., Theobalt, C., 2019. Real-time pose and shape reconstruction of two interacting hands with a single depth camera. ACM Transactions on Graphics 38, 1–13.

Neverova, N., Wolf, C., Nebout, F., Taylor, G.W., 2017. Hand pose estimation through semi-supervised and weakly-supervised learning. Computer Vision and Image Understanding 164, 56–67.

Panteleris, P., Oikonomidis, I., Argyros, A.A., 2018. Using a single rgb frame for real time 3d hand pose estimation in the wild, in: Proceedings of the IEEE Winter Conference on Applications of Computer Vision (WACV), pp. 436–445.

Paszke, A., Gross, S., Massa, F., Lerer, A., Bradbury, J., Chanan, G., Killeen, T., Lin, Z., Gimelshein, N., Antiga, L., Desmaison, A., Köpf, A., Yang, E., DeVito, Z., Raison, M., Tejani, A., Chilamkurthy, S., Steiner, B., Fang, L., Bai, J., Chintala, S., 2019. Pytorch: An imperative style, high-performance deep learning library, in: NeurIPS.

Pfister, T., Charles, J., Zisserman, A., 2015. Flowing convnets for human pose estimation in videos, in: Proceedings of the IEEE/CVF International Conference on Computer Vision (ICCV), pp. 1913–1921.

Qian, N., Wang, J., Mueller, F., Bernard, F., Golyanik, V., Theobalt, C., 2020. Html: A parametric hand texture model for 3d hand reconstruction and personalization, in: Proceedings of the European Conference on Computer Vision (ECCV), pp. 54–71.

Ramamoorthi, R., Hanrahan, P., 2001. An efficient representation for irradiance environment maps, in: Proceedings of the 28th annual conference on Computer graphics and interactive techniques (SIGGRAPH), pp. 497–500.

Ravi, N., Reizenstein, J., Novotny, D., Gordon, T., Lo, W.Y., Johnson, J., Gkioxari, G., 2020. Accelerating 3d deep learning with pytorch3d. arXiv preprint arXiv:2007.08501 .

Redmon, J., Farhadi, A., 2017. Yolo9000: Better, faster, stronger, in: Proceedings of the IEEE/CVF Conference on Computer Vision and Pattern Recognition (CVPR), pp. 6517–6525.

Romero, J., Tzionas, D., Black, M.J., 2017. Embodied hands: modeling and capturing hands and bodies together. ACM Transactions on Graphics 36, 245.

Rong, Y., Shiratori, T., Joo, H., 2021. Frankmocap: A monocular 3d whole-body pose estimation system via regression and integration, in: Proceedings of the IEEE/CVF International Conference on Computer Vision Workshops (ICCVW).

Shan, D., Geng, J., Shu, M., Fouhey, D.F., 2020. Understanding human hands in contact at internet scale, in: Proceedings of the IEEE/CVF Conference on Computer Vision and Pattern Recognition (CVPR), pp. 9866–9875.

Simon, T., Joo, H., Matthews, I., Sheikh, Y., 2017. Hand keypoint detec-

tion in single images using multiview bootstrapping, in: Proceedings of the IEEE/CVF Conference on Computer Vision and Pattern Recognition (CVPR), pp. 4645–4653.

Spurr, A., Dahiya, A., Zhang, X., Wang, X., Hilliges, O., 2021. Self-supervised 3d hand pose estimation from monocular rgb via contrastive learning, in: Proceedings of the IEEE/CVF International Conference on Computer Vision (ICCV), pp. 11210–11219.

Spurr, A., Iqbal, U., Molchanov, P., Hilliges, O., Kautz, J., 2020. Weakly supervised 3d hand pose estimation via biomechanical constraints., in: Proceedings of the European Conference on Computer Vision (ECCV), pp. 211–228.

Spurr, A., Song, J., Park, S., Hilliges, O., 2018. Cross-modal deep variational hand pose estimation, in: Proceedings of the IEEE/CVF Conference on Computer Vision and Pattern Recognition (CVPR), pp. 89–98.

Sun, Y., Bao, Q., Liu, W., Fu, Y., Black, M.J., Mei, T., 2021. Monocular, one-stage, regression of multiple 3d people, in: Proceedings of the IEEE/CVF International Conference on Computer Vision (ICCV), pp. 11159–11168.

Wan, C., Probst, T., Gool, L.V., Yao, A., 2019. Self-supervised 3d hand pose estimation through training by fitting, in: Proceedings of the IEEE/CVF Conference on Computer Vision and Pattern Recognition (CVPR), pp. 10845–10854.

Yang, L., Yao, A., 2019. Disentangling latent hands for image synthesis and pose estimation, in: Proceedings of the IEEE/CVF Conference on Computer Vision and Pattern Recognition (CVPR), pp. 9877–9886.

Yuan, S., Garcia-Hernando, G., Stenger, B., Moon, G., Chang, J.Y., Lee, K.M., Molchanov, P., Kautz, J., Honari, S., Ge, L., Yuan, J., Chen, X., Wang, G., Yang, F., Akiyama, K., Wu, Y., Wan, Q., Madadi, M., Escalera, S., Li, S., Lee, D., Oikonomidis, I., Argyros, A., Kim, T.K., 2018. Depth-based 3d hand pose estimation: From current achievements to future goals, in: Proceedings of the IEEE/CVF Conference on Computer Vision and Pattern Recognition (CVPR), pp. 2636–2645.

Zhang, J., Lin, L., Zhu, J., Hoi, S.C.H., 2021. Weakly-supervised multi-face 3d reconstruction. ArXiv abs/2101.02000.

Zhang, X., Huang, H., Tan, J., Xu, H., Yang, C., Peng, G., Wang, L., Liu, J., 2021. Hand image understanding via deep multi-task learning, in: Proceedings of the IEEE/CVF International Conference on Computer Vision (ICCV), pp. 11281–11292.

Zhang, X., Li, Q., Mo, H., Zhang, W., Zheng, W., 2019. End-to-end hand mesh recovery from a monocular rgb image, in: Proceedings of the IEEE/CVF International Conference on Computer Vision (ICCV), pp. 2354–2364.

Zhang, Y., You, S., Karaoglu, S., Gevers, T., 2022. Multi-person 3d pose estimation from a single image captured by a fisheye camera. Computer Vision and Image Understanding 222, 103505.

Zhou, X., Wang, D., Krähenbühl, P., 2019. Objects as points, in: arXiv preprint arXiv:1904.07850.

Zimmermann, C., Brox, T., 2017. Learning to estimate 3d hand pose from single rgb images, in: Proceedings of the IEEE/CVF International Conference on Computer Vision (ICCV), pp. 4913–4921.

Zimmermann, C., Ceylan, D., Yang, J., Russell, B., Argus, M.J., Brox, T., 2019. Freihand: A dataset for markerless capture of hand pose and shape from single rgb images, in: Proceedings of the IEEE/CVF International Conference on Computer Vision (ICCV), pp. 813–822.